# Astrophysically important $^{31}$S states studied with the $^{32}$S($p$, $d$)$^{31}$S reaction

Z. Ma,[1] D. W. Bardayan,[2] J. C. Blackmon,[2] R. P. Fitzgerald,[3] M. W. Guidry,[1] W. R. Hix,[2] K. L. Jones,[4] R. L. Kozub,[5] R. J. Livesay,[6] M. S. Smith,[2] J. S. Thomas,[4] and D. W. Visser[3]

[1]*Department of Physics and Astronomy, University of Tennessee, Knoxville, Tennessee 37996, USA*
[2]*Physics Division, Oak Ridge National Laboratory, Oak Ridge, Tennessee 37831, USA*
[3]*Department of Physics and Astronomy, University of North Carolina, Chapel Hill, North Carolina 27599, USA*
[4]*Department of Physics and Astronomy, Rutgers University, Piscataway, New Jersey 08854-8019, USA*
[5]*Physics Department, Tennessee Technological University, Cookeville, Tennessee 38505, USA*
[6]*Department of Physics, Colorado School of Mines, Golden, Colorado 80401, USA*

(Received 6 October 2006; revised manuscript received 3 May 2007; published 25 July 2007)

In nova outbursts on oxygen-neon white dwarfs, the $^{30}$P($p$, $\gamma$)$^{31}$S reaction plays a crucial role in the synthesis of heavier nuclear species, from Si to Ca. However, this important rate is very uncertain as a result of the lack of spectroscopic information on most of the levels above the proton threshold in $^{31}$S. To reduce these uncertainties, we have measured differential cross sections for the $^{32}$S($p$, $d$)$^{31}$S reaction and determined excitation energies for states in $^{31}$S. A total of 26 states in $^{31}$S were observed, including 17 above the proton threshold. Five new states were observed. Spins and parities were determined or constrained for 15 of the observed levels through a distorted wave Born approximation analysis of the angular distributions, of which six were made for the first time. We have evaluated 66 levels using existing data in combination with this measurement and calculated a new $^{30}$P($p$, $\gamma$)$^{31}$S reaction rate. We confirmed the spin-parity assignment of $1/2^+$ for the state at 6263 keV which dominates the $^{30}$P($p$, $\gamma$)$^{31}$S reaction rate at lower temperatures in novae, while the state at 6544 keV dominates at temperatures above 0.2 GK. Our results indicate that the $^{30}$P($p$, $\gamma$)$^{31}$S rate is reduced by up to a factor of 10 at nova temperatures compared to previous estimates.

DOI: 10.1103/PhysRevC.76.015803 PACS number(s): 27.30.+t, 25.40.Hs, 26.30.+k, 97.10.Cv

## I. INTRODUCTION

Classical novae occur in close binary systems consisting of a white dwarf and a companion main sequence star. When the companion star overflows its Roche lobe, matter from the star accumulates in an accretion disk before spiraling down onto the white dwarf. The temperature in the accumulated envelope increases because of gravitational compression. The inner layers of the accreted materials become partially degenerate. Material from the white dwarf core is mixed into the accreted hydrogen-rich layer through still uncertain mechanisms. When the temperature reaches ~20 million K, nuclear fusion reactions start and release a large amount of energy, further heating the envelope until a thermonuclear runaway is triggered. With peak temperatures up to 0.4 GK, the explosion ejects nuclear processed material into the interstellar medium which contributes to the galactic chemical evolution. In fact, classical nova outbursts have been proposed as the major source of the isotopes $^{13}$C, $^{17}$O, and perhaps $^{15}$N [1].

The study of nova nucleosynthesis is of considerable importance for several reasons. First, spectroscopic studies of the nova ejecta abundance pattern reveal the nature of the underlying white dwarf and provide information on the explosion such as its peak temperature. Explosions on carbon-oxygen white dwarfs (CO novae) are dominated by the synthesis of carbon-nitrogen-oxygen (CNO) group nuclei and thus result in an overproduction of these nuclei in the ejecta with respect to solar abundances [2]. The more massive oxygen-neon (ONe) novae contain not only CNO group nuclei but also Ne, Na, Al, and other intermediate-mass nuclei. Proton captures on these seed nuclei leaking out of the NeNa and MgAl cycles drive the nuclear activity up to the Si-Ca mass region [2]. Indeed, abundance determinations from some observed novae have shown the presence of enhanced Si-Ca nuclei in the ejecta [3,4]. Secondly, $\gamma$-ray emitting species are synthesized in nova outbursts and therefore are important for observational study of novae (Ref. [2] and references therein). Observations of $\gamma$ rays have been attempted with current satellites such as the International $\gamma$-Ray Astrophysics Laboratory (INTEGRAL) and will be made in the future with even more sensitive instruments [e.g., the Gamma-ray Large Area Space Telescope (GLAST)]. These emissions include a 478 keV line from $^{7}$Li, a 1275 keV line from $^{22}$Na, and a 511 keV line from $^{18}$F. In the Si-Ca region, $\gamma$-ray emission of 511 [5] and 2128 keV [6] lines from $\beta^+$ decay of the medium lived $^{34m}$Cl has been suggested. Particularly important is the observation of the 1809 keV line, signature of $^{26}$Al decay, which provided direct proof that nucleosynthesis is currently active in the Galaxy. Third, the discovery of several presolar grains of a nova origin characterized by low $^{12}$C/$^{13}$C and $^{14}$N/$^{15}$N ratios, high $^{26}$Al/$^{27}$Al ratio, close-to-solar $^{29}$Si/$^{28}$Si, and large excesses in $^{30}$Si/$^{28}$Si [7] points out the importance of precise determinations of the abundance patterns and nova nucleosynthesis, in particular for the Si-Ca mass region.

There have been previous studies of nova nucleosynthesis in the Si-Ca mass region using calculations coupling hydrodynamics and nuclear reactions [2,8,9]. José *et al.* [2] was the first to point out that the $^{30}$P($p$, $\gamma$)$^{31}$S reaction rate plays a crucial role in the synthesis of heavier nuclear species—from Si to Ca—in nova outbursts on ONe white dwarfs. Species beyond sulfur are produced

 ©2007 The American Physical Society

via two paths, either $^{30}P(p,\gamma)^{31}S(p,\gamma)^{32}Cl(\beta^+)^{32}S$ or $^{30}P(p,\gamma)^{31}S(\beta^+)^{31}P(p,\gamma)^{32}S$. Other paths are suppressed. For example, the path through $^{29}P(p,\gamma)^{30}S(p,\gamma)^{31}Cl$ is inhibited by the instant inverse photodisintegration reaction $^{31}Cl(\gamma,p)^{30}S$, followed rapidly by a $\beta^+$ decay leading back to $^{30}P$. The path through $^{30}P(\beta^+)^{30}Si(p,\gamma)^{31}P(p,\gamma)^{32}S$ is also strongly inhibited by the slow (2.498 min) $^{30}P$ $\beta^+$ decay. Thus $^{30}P(p,\gamma)^{31}S$ is a gateway reaction to synthesize isotopes beyond sulfur. José *et al.* varied the $^{30}P(p,\gamma)^{31}S$ reaction rate within its uncertainty [2] to explore its effects on nova nucleosynthesis. The increase by a factor of 100 significantly affects only the $^{30}Si$ yield, and since the path toward $^{31}S$ is favored, much less $^{30}Si$ is left in the envelope. The impact on the other nuclear species is very limited. This indicates that the $^{30}P(p,\gamma)^{31}S$ rate is estimated to be significantly faster than competing reactions. On the contrary, a reduction by a factor of 100 of the $^{30}P(p,\gamma)^{31}S$ rate changes the expected yields dramatically. Since $^{30}P$ $\beta^+$ decays compete favorably with proton captures, an important enhancement of $^{30}Si$ is obtained. More importantly, however, the synthesis of elements above Si is hindered significantly by a factor of 10 with respect to values found with the nominal rate. Iliadis *et al.* [8] performed one-zone post-processing nucleosynthesis calculations to investigate the effects of thermonuclear reaction rate uncertainties on nova nucleosynthesis. They found qualitative and quantitative agreement with José *et al.* We performed post-processing nova nucleosynthesis simulations based on a multiple spatial zones model [9,10]. The influence of the $^{30}P(p,\gamma)^{31}S$ rate on nova nucleosynthesis found in our calculations agrees well with previous studies.

Direct measurement of the $^{30}P(p,\gamma)^{31}S$ reaction rate has not yet been possible because of difficulties in developing radioactive $^{30}P$ beams. The currently adopted rate is based on a statistical Hauser-Feshbach calculation [11], and it has an uncertainty that could be as high as a factor of 100 up or down [12]. This is because such calculations are generally valid at temperatures higher than those reached in novae, and they do not treat individual resonances which may dominate the rate at lower temperatures. Unfortunately, the lack of spectroscopic information on most proton unbound $^{31}S$ states makes it difficult to calculate a realistic reaction rate. Before the present work was begun, there were 17 levels known in the compilation [13] above the proton threshold up to 1 MeV that may contribute to the $^{30}P(p,\gamma)^{31}S$ reaction rate at nova temperatures, but very few have assigned spins and parities. A recent work [14] measured five levels (one new) with a fusion evaporation reaction and evaluated [15] nine more levels. To clarify the level structure of $^{31}S$ above the proton threshold and to reduce the uncertainty in calculating the $^{30}P(p,\gamma)^{31}S$ rate, we have measured the single-particle transfer reaction $^{32}S(p,d)^{31}S$. Angular and energy distributions of deuterons were obtained for several states and used to deduce the spectroscopic information on $^{31}S$ levels.

## II. EXPERIMENTAL PROCEDURE

A 32 MeV proton beam from the 25 MeV tandem accelerator at the ORNL Holifield Radioactive Ion Beam Facility (HRIBF) was used to bombard a ZnS target. Deuterons from the $^{32}S(p,d)^{31}S$ reaction were detected at forward angles in the silicon detector array (SIDAR) [17], an annular array of silicon strip detectors. Each detector is segmented into 16 radial strips which allows the extraction of angular distribution information. The SIDAR provides large solid angle coverage and excellent energy resolution. The high segmentation allows a higher counting rate without pileup than could be obtained with a single detector of the same area. The deuterons were distinguished from the other reaction products observed (protons, tritons) by running the SIDAR in "telescope" mode with 300-$\mu$m-thick $\Delta E$ detectors backed by 500-$\mu$m-thick $E$ detectors and using the standard $\Delta E$-$E$ techniques (Fig. 1). In one set of runs, the SIDAR was arranged to cover laboratory angles 17°–48°, and a ZnS target with a thickness of 285 $\mu$g/cm$^2$ deposited on 1 $\mu$g/cm$^2$ carbon backing was used. This arrangement ensured a coverage of the $^{31}S$ excitation energies ranging from 4–11 MeV. In a second set of runs, the SIDAR was arranged to cover 31°–75°, and a 280 $\mu$g/cm$^2$ ZnS target with 5 $\mu$g/cm$^2$ carbon backing was used. The five times increase in the backing brought substantially more background in this set of runs, however. The energy resolution obtained for the first set of runs was $\Delta E_{\text{c.m.}} \sim 80$ keV, and $\Delta E_{\text{c.m.}} \sim 130$ keV for the second set of runs where the loss of resolution in the second set was due to the greater kinematic broadening at the larger angles covered by the SIDAR. Because of the considerably better energy resolution and lower background contamination in the first set, excitation energies were extracted from these data whenever possible. For the purposes of energy calibration and background identification, another set of runs was taken with a 250 $\mu$g/cm$^2$ Zn target on a 11 $\mu$g/cm$^2$ parylene ($C_8H_8$) backing over the same angles as the first set of runs. However, we did not observe noticeable groups from zinc isotopes. The five deuteron groups observed in the background runs were identified with the four lowest levels in $^{11}C$ from the $^{12}C(p,d)^{11}C$ reaction and the 6176 keV level in $^{15}O$ from the $^{16}O(p,d)^{15}O$ reaction. The beam current was integrated downstream from the target chamber using a thick graphite beam stop.

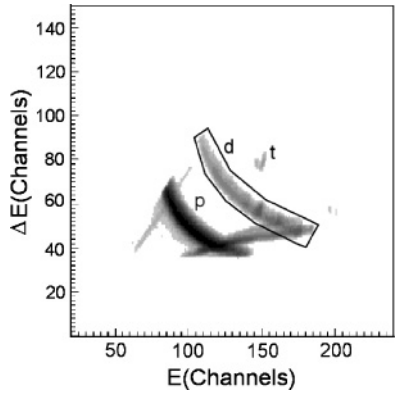


FIG. 1. Energy loss $\Delta E$ vs total energy $E$ spectrum for the SIDAR. Deuterons corresponding to excitation energies 4–11 MeV were stopped.

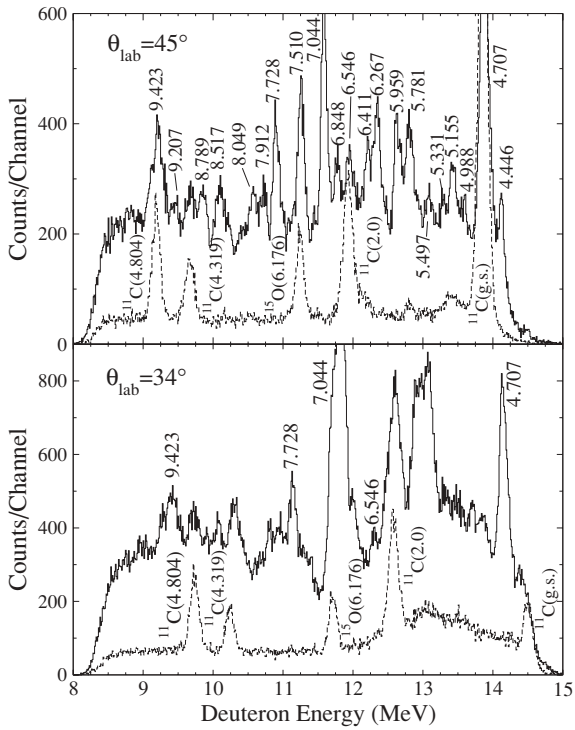


FIG. 2. Representative deuteron energy spectra from reactions on the ZnS target are shown as solid lines and those from Zn + $C_8H_8$ target as dashed lines. The peaks from $^{32}S(p,d)^{31}S$ are labeled by their excitation energies extracted in this measurement.

## III. EXPERIMENTAL RESULTS AND DISCUSSION

### A. EXCITATION ENERGIES

Representative energy spectra for the deuterons gated on the $\Delta E$-$E$ spectrum (see Fig. 1) are plotted in Fig. 2 for both the data runs and the background runs. The energy calibration was obtained for each of the 16 observed laboratory angles using the data from the background runs, where the deuteron spectra were taken under identical experimental conditions as in the data runs, only changing the target. We have used the four deuteron groups from the $^{12}C(p,d)^{11}C$ reaction in the background spectra to establish a correlation between measured channels and deuteron energies. These four groups were identified with the ground state and first three excited states of $^{11}$C whose excitation energies are well known, and the values span almost the total range of interest of deuteron energies for the $^{32}S(p,d)^{31}S$ measurement. At each angle, the centroids of these peaks were extracted and fitted to the expected deuteron energies from kinematics. For most cases the fits reproduced the expected deuteron energies to within ±8 keV. These calibrations were used to deduce the deuteron energies from the $^{32}S(p,d)^{31}S$ reaction. The deuteron energies were then converted to excitation energies, and adopted values were obtained by averaging the excitation energies extracted for each angle.

The uncertainty for each of the averaged excitation energies was calculated using the standard formalism [18]. Additional sources of uncertainty listed below were considered but found to be negligible [16]. The beam energy has been calibrated to 1/10 000 [19] and has been checked on numerous occasions (e.g., Ref. [17]). For deuterons detected in our experiment with energies around 8–15 MeV, the energy losses in targets were only a few keV, and the uncertainties resulting from these small corrections between the two targets were negligible. The angles covered by the SIDAR were calculated from the known detector geometry and were cross-checked by noting the relative difference of the energy dependence on angle between deuterons from $^{32}S(p,d)^{31}S$ and $^{12}C(p,d)^{11}C$ reactions. All these uncertainties were found negligible compared to the statistical uncertainties.

The excitation energies that we extracted for the states in $^{31}$S are labeled in Fig. 2 and listed in Table I. A total of 26 energy levels were observed, of which five states at 8789, 9207, 9606, 9853, and 10577 keV had not been previously reported. Uncertainties in the excitation energies of states in the high energy region were significantly reduced from previous measurements. Our excitation energies agree well with previous measurements [14,20–25].

### B. SPIN AND PARITY ATTRIBUTIONS

Angular distributions were extracted for strongly populated states and are plotted in Fig. 3. Gaps appear in the angular distributions where the peak of interest was obscured by contaminant peaks from background reactions. The overall normalization of our cross section data was not well determined because of uncertainties in target stoichiometry and beam current integration. However, this uncertainty has no effect on our conclusions concerning the excitation energies and spins of $^{31}$S levels. The cross sections measured by Kozub [26] at 33.6 MeV proton energy should be ∼10% higher than our 32 MeV measurements. Taking this small difference into account, we have normalized our angular distributions to the data in Ref. [26] and used this normalization to extract spectroscopic factors.

To analyze the experimentally measured angular distributions, finite range distorted-wave Born approximation (DWBA) calculations were performed, using the computer code DWUCK5 [27]. We used optical model and bound state parameters from the previous $^{32}S(p,d)^{31}S$ study [26], which are given in Table II. These parameters have resulted in good fits to the observed angular distributions (Fig. 3). The observed transitions exhibit angular distributions whose shapes strongly depend on $\ell_n$-transfer values. An $\ell_n = 0$ transfer would lead to an unambiguous assignment of spin-parity $1/2^+$ to the final state in $^{31}$S, since the target $^{32}$S is an even-even $0^+$ nucleus. For $\ell_n = 1$ or $\ell_n = 2$ transfers, since the angular distributions depend very weakly on the total angular momentum, we could not differentiate between $\ell_n+1/2$ and $\ell_n-1/2$ transitions. The plotted transitions shown on Fig. 3 are for $1p_{1/2}$ and $1d_{5/2}$ transfers, respectively. The proposed spin and parity assignments for all the levels observed in the present measurement are listed in Table I and discussed below. Levels not observed in our measurement but which lie within 1 MeV above the proton threshold that may contribute to the $^{30}P(p,\gamma)^{31}S$ reaction rate are also discussed. In total,

TABLE I. Excitation energies (in keV) of $^{31}$S states extracted from this measurement compared with previously reported values. Present evaluation of excitation energies is based on P. M. Endt's previous evaluation [13] and experimental information on $^{31}$S levels thereafter as listed in columns 3–6 (see Ref. [14,24,25]). $J^\pi$ values are assigned based on the present measurement and previous studies. Neutron spectroscopic factors $C^2S$ from present work and a previous neutron pickup study of $^{32}$S($^3$He,$\alpha$)$^{31}$S [24] are listed in the last two columns. $^{31}$P mirror states are also listed.

| Present evaluation | Ref. [13] Endt | Ref. [24] $^{32}$S($^3$He,$\alpha$) ($\pm$5 kev) | Ref. [14] $^{12}$C($^{20}$Ne,$n\gamma$) | Ref. [25] $^{31}$Cl $\beta$ decay | This work $^{32}$S($p$, $d$) | $\ell_n$ | $J^\pi$ | $^{31}$P mirror | $C^2S$ | $C^2S$ |
|---|---|---|---|---|---|---|---|---|---|---|
| 4085 ± 2 | 4080 ± 8 | 4087 | | | 4085 ± 2 | 2 | $5/2^+$ | 4190 | 0.77 | 0.91 |
| 4204 ± 7 | 4204 ± 7 | | | | | | $(1/2-7/2)^+$ | | | |
| 4450.9 ± 0.4 | 4452 ± 6 | 4451 | 4450.9 ± 0.4 | | 4446 ± 6 | 3 | $7/2^-$ | 4431 | 0.15 | 0.22 |
| 4525 ± 8 | 4525 ± 8 | | | | | | $3/2^+$ | | | |
| 4583.8 ± 0.3 | 4580 ± 6 | 4579 | 4583.8 ± 0.3 | | | | $7/2^+$ | | | 0.10 |
| 4712 ± 2 | 4718 ± 6 | 4720 | | | 4707 ± 3 | 2 | $5/2^+$ | 4783 | 0.40 | 0.38 |
| 4866 ± 7 | 4866 ± 7 | | | | | | | | | |
| 4976 ± 4 | 4969 ± 7 | 4975 | | | 4988 ± 8 | | $3/2^-$ | 5015 | | 0.04 |
| 5027 ± 5 | 5022 ± 12 | 5028 | | | | | | | | |
| 5156 ± 3 | 5151 ± 6 | 5161 | | | 5155 ± 5 | 0 | $1/2^+$ | 5256 | 0.11 | 0.10 |
| 5300.6 ± 0.3 | 5306 ± 9 | 5305 | 5300.5 ± 0.3 | | 5331 ± 5 | | $9/2^+$ | 5343 | | |
| 5408 ± 9 | 5408 ± 9 | | | | | | | | | |
| 5440 ± 11 | 5440 ± 11 | | | | | | | | | |
| 5515 ± 4 | 5515 ± 11 | 5519 | | | 5497 ± 10 | 2 | $3/2^+$ | 5559 | 0.10 | |
| 5679 ± 4 | 5685 ± 8 | 5677 | | | | | | | | |
| 5774 ± 2 | 5781 ± 8 | 5777 | | 5772 ± 2 | 5781 ± 5 | 2 | $5/2^+$ | 5892 | 0.17 | 0.17 |
| 5826 ± 10 | 5826 ± 10 | | | | | | | | | |
| 5890 ± 4 | 5894 ± 9 | 5889 | | | 5959 ± 10[a] | 2 | $(3/2, 5/2)^+$ | | 0.15 | 0.12 |
| 5977.7 ± 0.7 | 5985 ± 10 | 5975 | 5977.7 ± 0.7 | | 5959 ± 10[a] | 2 | $(9/2^+)$ | | | 0.20 |
| 6160.2 ± 0.7 | 6155 ± 10 | | 6160.2 ± 0.7 | | | | $5/2^-$ | 6399 | | |
| 6263 ± 3 | 6267 ± 10 | 6257 | | | 6267 ± 5 | 0 | $1/2^+$ | 6337 | 0.12 | 0.17 |
| 6280 ± 2 | 6268 ± 10 | | | 6280 ± 2 | | | $3/2^+$ | 6381 | | |
| 6350 ± 11 | 6350 ± 11 | | | | | | $5/2^+$ | 6461 | | |
| 6376.9 ± 0.5 | | | 6376.9 ± 0.5 | | | | $9/2^-$ | 6501 | | |
| 6393.8 ± 0.5 | 6396 ± 10 | 6393 | 6393.7 ± 0.5 | | 6411 ± 9 | | $11/2^+$ | 6454 | | |
| 6544 ± 9 | 6543 ± 11 | | | | 6546 ± 15 | | $5/2^-$ | 6594 | | |
| 6593 ± 15 | 6593 ± 15 | | | | | | $3/2^-$ | 6610 | | |
| 6636.2 ± 1.5 | 6628 ± 13 | | 6636.3 ± 1.5 | | | | $9/2^-$ | 6793 | | |
| 6712 ± 11 | 6712 ± 11 | | | | | | $(3/2-7/2)$ | | | |
| 6748 ± 10 | 6748 ± 10 | | | | | | $(3/2-7/2)$ | | | |
| 6796 ± 25 | 6796 ± 25 | | | | | | $(3/2-7/2)$ | | | |
| 6833.4 ± 0.3 | 6835 ± 9 | | 6833.4 ± 0.3 | | 6848 ± 9[a] | | $11/2^-$ | 6825 | | |
| 6870 ± 10 | 6870 ± 10 | | | | 6848 ± 9[a] | | $(3/2^-, 5/2^+)$ | 7080 | | |
| 6921 ± 13 | 6921 ± 25 | | | 6921 ± 15 | | | $5/2^+$ | 6932 | | |
| 6970 ± 5 | 6990 ± 20 | 6966 | | 7015 ± 19 | | | $1/2^+$ | | | 0.02 |
| 7006 ± 25 | 7006 ± 25 | | | | | | $1/2^+$ | | | |
| 7038 ± 4 | 7039 ± 10 | 7033 | | | 7044 ± 6 | 2 | $5/2^+$ | 7158[b] | 0.79 | 0.76 |
| 7112 ± 25 | 7112 ± 25 | | | | | | $(1/2, 3/2)^-$ | 7214 | | |
| 7155 ± 4 | 7155 ± 9 | 7156 | | 7144 ± 16 | | | $(3/2, 5/2)^+$ | | | 0.11 |
| 7199 ± 13 | 7199 ± 13 | | | | | | | | | |
| 7303.2 ± 0.7 | 7310 ± 11 | | 7303.1 ± 0.7 | 7348 ± 20 | | | $11/2^+$ | | | |
| 7445 ± 25 | 7445 ± 25 | | | | | | | | | |
| 7511 ± 5 | 7522 ± 20 | | | | 7510 ± 6 | | | | | |
| 7600 ± 30 | 7600 ± 30 | | | | | | | | | |
| 7660 ± 30 | 7660 ± 30 | | | | | | | | | |
| 7726 ± 3 | 7715 ± 15 | 7725 | | 7705 ± 21 | 7728 ± 4 | 0 + 2 | | | | |
| 7768 ± 25 | 7768 ± 25 | | | | | | | | | |
| 7850 ± 25 | 7850 ± 25 | | | | | | | | | |
| 7910 ± 5 | 7888 ± 25 | | | 7878 ± 23 | 7912 ± 5 | 0 | $1/2^+$ | | 0.06 | |
| 8003 ± 17 | 7985 ± 25 | | | 8019 ± 24 | 8049 ± 6[a] | 0 + 2 | $(1/2, 3/2, 5/2)^+$ | | | |
| 8082 ± 25 | 8082 ± 25 | | | | 8049 ± 6[a] | 0 + 2 | $(1/2, 3/2, 5/2)^+$ | | | |

TABLE I. *(Continued.)*

| Present evaluation | Ref. [13] Endt | Ref. [24] $^{32}$S($^3$He,$\alpha$) ($\pm$5 kev) | Ref. [14] $^{12}$C($^{20}$Ne,$n\gamma$) | Ref. [25] $^{31}$Cl $\beta$ decay | This work $^{32}$S($p$, $d$) | $\ell_n$ | $J^\pi$ | $^{31}$P mirror | $C^2S$ | $C^2S$ |
|---|---|---|---|---|---|---|---|---|---|---|
| 8174 $\pm$ 11 | 8183 $\pm$ 25 | | | | 8171 $\pm$ 12 | | | | | |
| 8328 $\pm$ 19 | 8362 $\pm$ 25 | | | 8278 $\pm$ 30 | | | | | | |
| 8461.6 $\pm$ 0.5 | 8453 $\pm$ 25 | | 8461.6 $\pm$ 0.5 | 8425 $\pm$ 30 | | | (13/2$^-$) | | | |
| 8515 $\pm$ 12 | | | | 8509 $\pm$ 30 | 8517 $\pm$ 13 | 0 | 1/2$^+$ | | 0.05 | |
| 8669 $\pm$ 40 | | | | 8669 $\pm$ 40 | | | | | | |
| 8789 $\pm$ 6 | | | | | 8789 $\pm$ 6 | 2 | (3/2, 5/2)$^+$ | | 0.13 | |
| 8821 $\pm$ 40 | | | | 8821 $\pm$ 40 | | | | | | |
| 8977 $\pm$ 40 | | | | 8977 $\pm$ 40 | | | | | | |
| 9154.4 $\pm$ 1.2 | | | 9154.4 $\pm$ 1.2 | | | | 13/2$^+$ | | | |
| 9207 $\pm$ 5 | | | | | 9207 $\pm$ 5 | | | | | |
| 9423 $\pm$ 7 | | | | | 9423 $\pm$ 7 | 2 | (3/2, 5/2)$^+$ | | 0.19 | |
| 9606 $\pm$ 14 | | | | | 9606 $\pm$ 14 | | | | | |
| 9853 $\pm$ 12 | | | | | 9853 $\pm$ 12 | | | | | |
| 10146.3 $\pm$ 1.0 | | | 10146.3 $\pm$ 1.0 | | | | (13/2$^-$) | | | |
| 10577 $\pm$ 13 | | | | | 10577 $\pm$ 13 | | | | | |

[a]Unresolved doublets.
[b]See Ref. [24].

we evaluate the properties of 44 levels in $^{31}$S. Identification of mirror states in $^{31}$P and $^{31}$S are based on previous studies [13,14,24] and present experimental information. Identification of several other pairs of levels as mirror states was also attempted considering two criteria: similarity of the excitation energies and consistency of the $J^\pi$ values [24]. The validity of these criteria has been demonstrated in previous works (e.g., Refs. [13,14,24]).

Neutron spectroscopic factors $C^2S$ were extracted by comparison of our experimental angular distributions with the results of DWUCK5 calculations and are also listed in Table I. By normalizing our cross sections to those of Ref. [26], as discussed above, we obtain spectroscopic factors in good agreement with values from previous neutron pickup studies (see Ref. [24] and references therein).

*4085 keV level*. This level has been reported to have $J^\pi = (3/2, 5/2)^+$ [13] deduced from various transfer reaction studies [22,26,28]. Vernotte *et al*. reported this level to have $J^\pi = 5/2^+$ on the basis of a $^{32}$S($^3$He,$\alpha$)$^{31}$S study [24]. The combined angular distribution from present work and Kozub's [26] previous measurement is well fit by an $\ell_n = 2$ transfer and thus supports this assignment. This level was identified as being the mirror of the $^{31}$P state at 4190 keV with $J^\pi = 5/2^+$ [13,24].

*4451 keV level*. This level is given an assignment of (5/2,7/2)$^-$ in Ref. [13] obtained from a $^{32}$S($^3$He,$\alpha$)$^{31}$S study [23]. Vernotte *et al*. [24] reported this level to have a 7/2$^-$ assignment. A $^{12}$C($^{20}$Ne,$n\gamma$)$^{31}$S study by Jenkins *et al*. [14] yielded the same $J^\pi$ of 7/2$^-$. In our measurement the angular distribution is reasonably well reproduced by an $\ell_n = 3$ transfer. The present assignment is $J^\pi = 7/2^-$. It was identified with the 4431 keV 7/2$^-$ level in $^{31}$P [13,24].

*4712 keV level*. In the adopted level scheme [13] this level is assigned $J^\pi = (3/2, 5/2)^+$ [13] obtained from ($^3$He,$\alpha$) [21] and ($p$, $t$) [28] studies. Vernotte *et al*. [24] assigned 5/2$^+$ to the level at 4720 keV. In our case this level is strongly populated. The combined angular distribution from our data and Kozub's previous measurement [26] is well reproduced by an $\ell_n = 2$ transfer with a small component of $\ell_n = 0$ admixture to account for the rise at small angles. Based on present work and previous measurements this level is assigned with $J^\pi = 5/2^+$. It has been identified with the 4783 keV 5/2$^+$ mirror state in $^{31}$P [13,24].

*4976 keV level*. The level at 4969 keV in the adopted level scheme [13] was assigned a $J^\pi = (1/2, 3/2)^-$ from a $^{32}$S($^3$He,$\alpha$)$^{31}$S study [23]. This is supported by Vernotte *et al*. [24] in their ($^3$He,$\alpha$) measurement with an $\ell_n = 1$ neutron pickup. In our experiment this level is only weakly populated, and we could not extract an angular distribution. In Ref. [24] it was identified as the mirror of the 3/2 state in $^{31}$P at 5014.9 keV and assigned with 3/2$^-$.

TABLE II. Potential parameters used in DWBA calculations for the $^{32}$S($p$, $d$)$^{31}$S reaction.

| Particle | $V_R$ (MeV) | $r_R$ (fm) | $a_R$ (fm) | $4W_D$ (MeV) | $r_I$ (fm) | $a_I$ (fm) | $r_c$ (fm) | $\lambda_{SO}$ |
|---|---|---|---|---|---|---|---|---|
| $p$ | 47.1 | 1.18 | 0.66 | 27.5 | 1.18 | 0.66 | 1.18 | |
| $d$ | 90.0 | 1.25 | 0.62 | 100.0 | 1.30 | 0.58 | 1.18 | |
| $n$ | 56.0 | 1.20 | 0.65 | | | | | 251[a] |

[a]Thomas spin-orbit factor.

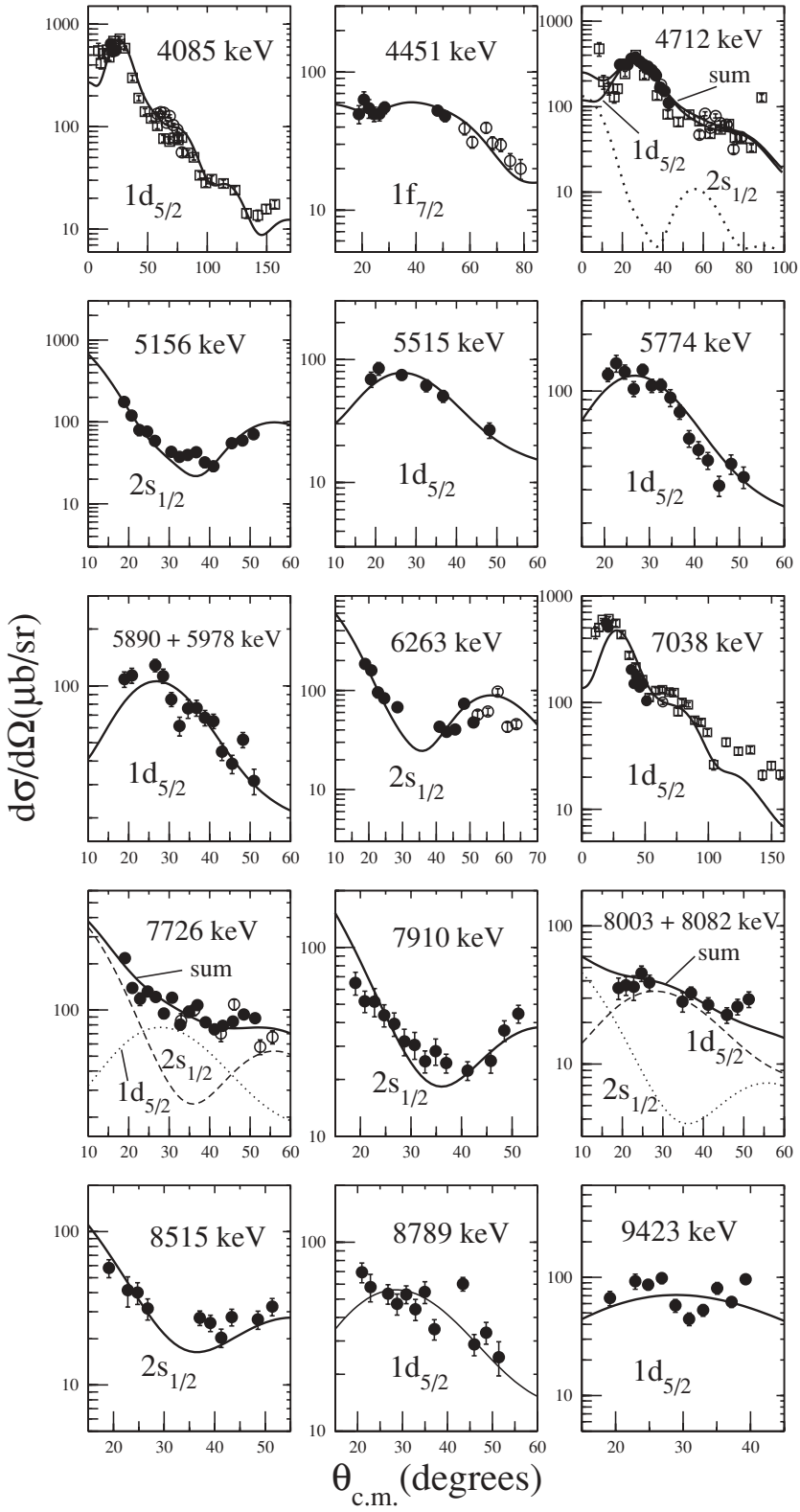


FIG. 3. Angular distributions for data from the first set of runs (filled circles), from the second set of runs (empty circles), and from Kozub [26] (squares). If not shown, the error is smaller than the point size. Our DWBA calculations best fitting the observed angular distributions are also shown.

*5156 keV level.* The 5156 keV state was reported to be a $1/2^+$ [13], and it was confirmed by Vernotte *et al.* [24]. In our measurement the extracted angular distribution was well reproduced by an $\ell_n = 0$ transfer leading to an unambiguous $1/2^+$ assignment. This level is the mirror state of the 5256 keV level in $^{31}$P.

*5301 keV level.* We could not extract an angular distribution for this state because of its relatively weak population. It was reported to be a $9/2^+$ level in Ref. [14]. This large spin value explains the weak population in the present experiment, as the $(p, d)$ reaction prefers a small angular momentum transfer. Based on the similarity of the excitation energies

and consistency of the $J^\pi$ values, we identify this level as the mirror of the 5343 keV level in $^{31}$P with $J^\pi = 9/2^+$ [14].

*5515 keV level*. This level had not previously been given an assignment. In our measurement this level is quite weakly populated and the extracted angular distribution is compatible with an $\ell_n = 2$ transition which leads to an assignment of $J^\pi = (3/2, 5/2)^+$. Moss [23] has found possible presence of $\ell_n = 3$ component but it appears unlikely in our case. We tentatively identified it as being the mirror of the 5559 keV level in $^{31}$P with $J^\pi = 3/2^+$ based on similar excitation energies and spins.

*5774 keV level*. This level was given an assignment of $J^\pi = (3/2, 5/2)^+$ [13] resulting from an $\ell_n = 2$ transfer in a $^{32}$S($^3$He,$\alpha$)$^{31}$S study [21]. Vernotte *et al*. [24] identified this level with the 5892 keV in $^{31}$P and assigned both levels with $5/2^+$. Kankainen *et al*. [25] observed this level at 5772 $\pm$ 2 keV in a $^{31}$Cl $\beta$-decay study. In our measurement this level is reasonably populated, and the angular distribution was well fit by an $\ell_n = 2$ transfer and thus supports the $5/2^+$ assignment.

*5890 and 5978 keV levels*. The states at 5894 and 5985 keV in the adopted level scheme [13] were not separated in our study. It had been reported that the higher-energy level was a $9/2^+$ state [14]. The lower-energy level was assigned a $J^\pi = (3/2, 5/2)^+$ based on an $\ell_n = 2$ transfer in $^{32}$S($^3$He,$\alpha$)$^{31}$S studies [21,24]. Our extracted angular distribution is well fit by an $\ell_n = 2$ transition and thus supports this assignment.

*6160 keV level*. This level was not observed in our measurement. Jenkins *et al*. [15] reported this level at 6160 keV and identified this level as the mirror of the $J^\pi$ $5/2^-$ state in $^{31}$P at 6399 keV on the basis of their very similar decay branches.

*6263 keV level*. The 6263 keV state has been assigned spin and parity quantum numbers of $1/2^+$ and identified as the mirror partner of the 6337 keV state in $^{31}$P [13,24]. In the present measurement this level was reasonably populated and the angular distribution was well fit by an $\ell_n = 0$ transfer, and thus confirmed the unambiguous $J^\pi$ $1/2^+$ assignment.

*6280 keV level*. The level at 6268 keV in Ref. [13] is not expected to be populated in our $^{32}$S($p, d$)$^{31}$S measurement since it is known to have isospin $T = 3/2$. Kankainen *et al*. [25] deduced a more precise excitation energy of 6280 $\pm$ 2 keV in their $^{31}$Cl $\beta$-decay study. It is the mirror state of the $T = 3/2$ 6381 keV level in $^{31}$P ($J^\pi = 3/2^+$). We do not expect a strong contribution to the $^{30}$P($p, \gamma$)$^{31}$S rate from this $T = 3/2$ state by proton capture on a $T = 0$ ground state of $^{30}$P.

*6350 keV level*. The 6350 keV level was not observed in the present measurement. In their $^{29}$Si($^3$He,$n$)$^{31}$S study [22], Davidson *et al*. found this state well populated through $L = 2$ transfer. This would allow $J^\pi = (3/2, 5/2)^+$ assignment for the 6350 keV level. We tentatively link it as the mirror of the $5/2^+$ state in $^{31}$P at 6461 keV based on similarity in excitation energies and consistency in $J^\pi$ values.

*6377 keV level*. This level was only observed in Ref. [14] and was assigned a $J^\pi = 9/2^-$.

*6394 keV level*. This level was observed by Jenkins *et al*. [14] with an assignment of $J^\pi = 11/2^+$, and was identified with the $11/2^+$ level in $^{31}$P at 6454 keV. We could not extract an angular distribution because of its weak population. The contribution of this level to the $^{30}$P($p, \gamma$)$^{31}$S rate is negligible for an $\ell_p = 4$ proton capture.

*6544 and 6593 keV levels*. The 6544 keV level was only observed at two angles, and the 6593 keV level was not observed in the present work. They were proposed by Jenkins *et al*. [15] to have $J^\pi = 5/2^-$ and $3/2^-$, respectively.

*6636 keV level*. This level was not observed in our study. It was observed by Jenkins *et al*. [15] and was proposed as the analog of the $9/2^-$ state in $^{31}$P at 6793 keV on the basis of similar $\gamma$-decay schemes.

*6712, 6748, and 6796 keV levels*. These three states were not observed in the present work. Jenkins *et al*. [15] tentatively proposed these levels to have $J^\pi = (3/2 - 7/2)$ assignments.

*6833 and 6870 keV levels*. The previously reported states at 6835 and 6870 keV [13] were not separated in our study. The centroid of the combined peak was found at 6848 keV. In their $^{12}$C($^{20}$Ne,$n\gamma$)$^{31}$S study, Jenkins *et al*. [14] observed a 6833 keV level with $J^\pi = 11/2^-$, and identified it as the mirror of the $11/2^-$ state in $^{31}$P at 6825 keV. They assigned the 6870 keV level with $J^\pi = (3/2^-, 5/2^+)$ [15].

*6921 keV level*. The 6921 keV level was observed previously in a $^{29}$Si($^3$He,$n$)$^{31}$S study [22] and a $^{31}$Cl $\beta$-decay study [25] without spin and parity assigned. We do not observe this level in the present work. Based on similarity of the excitation energies and consistency of the $J^\pi$ values, this level is likely the analog of the 6932 keV state in $^{31}$P with $J^\pi = 5/2^+$.

*6970 and 7006 keV levels*. In the adopted level scheme [13] they were considered as one level, which is the mean value of three levels obtained from various sources. The level observed in the $^{29}$Si($^3$He,$n$)$^{31}$S reaction [22] ($E_x$ = 7006 keV, $J^\pi = 1/2^+$) was identified as being the second $T = 3/2$ state of $^{31}$S, and thus a significant contribution to the $^{30}$P($p, \gamma$)$^{31}$S reaction rate is not expected. Vernotte *et al*. [24] pointed out that since the population of a $T = 3/2$ state through the $^{32}$S($^3$He,$\alpha$)$^{31}$S reaction [20,21] is isospin forbidden, the presence of two distinct levels at 6990 and 7006 keV, respectively, was assumed. They also observed the lower level at 6966 keV and assigned it with $J^\pi = 1/2^+$. Kankainen *et al*. [25] observed this level at 7015 $\pm$19 keV in their $^{31}$Cl $\beta$-decay study.

*7038 keV level*. This level has been reported previously to have $J^\pi = (3/2, 5/2)^+$ [13]. Vernotte *et al*. [24] assigned it with $J^\pi = 5/2^+$ and identified it with a $^{31}$P level at 7158 keV. The angular distribution extracted in our study combined with data from a previous ($p, d$) measurement [26] was well fit by an $\ell_n = 2$ transfer and thus supports the $5/2^+$ assignment.

*7112 keV level*. We do not observe this level in the present work. It was only previously reported in a $^{29}$Si($^3$He,$n$)$^{31}$S reaction [22] without spin and parity assignment. To calculate its possible contribution to the $^{30}$P($p, \gamma$)$^{31}$S rate, we tentatively identify it as being the analog of the $J^\pi = (1/2, 3/2)^-$ state in $^{31}$P at 7214 keV based on similarity in excitation energies and consistency of the $J^\pi$ values.

*7155 keV level*. The 7155 keV level was not observed in our measurement. It was previously given a $J^\pi = (3/2, 5/2)^+$ assignment on the basis of an $\ell_n = 2$ transition in a $^{32}$S($^3$He,$\alpha$)$^{31}$S study [21]. Vernotte *et al*. [24] supported this assignment.

*7303 keV level*. This level was not observed in the present measurement. Jenkins *et al*. [14] observed it at 7303 keV with $J^\pi = 11/2^+$.

*7511 keV level*. This level was previously only observed by F. Ajzenberg-Selove *et al*. [20]. It was quite weakly populated in the present measurement, and a reasonable angular distribution could not be extracted.

*7726 keV level*. This level was previously reported by J. Aysto *et al*. [29] and Kankainen *et al*. [25] to have $J^\pi = (1/2 \text{ to } 5/2)^+$ assignment. Vernotte *et al*. [24] observed a broad peak at 7725 keV, and they fitted the angular distribution by a superposition of $\ell_n = 1$ and 2 transitions, or $\ell_n = 1$ and 3 transitions. They thus considered this level a combination of several levels. The angular distribution we extracted is best fit by a combination of $\ell_n = 0 + 2$ transfers.

*7910 keV level*. A level at 7888 keV was reported by Davidson *et al*. [22]. Källne and Fagerström reported a $7970 \pm 70$ keV level in a $^{32}$S$(p, d)^{31}$S study [30]. Kankainen *et al*. [25] observed it at $7878 \pm 23$ keV in their $^{31}$Cl $\beta$-decay study. We observed this level at 7912 keV and extracted an angular distribution best reproduced by an $\ell_n = 0$ angular momentum transfer, and assigned spin and parity $1/2^+$.

*8003 and 8082 keV levels*. These two levels are not separated in our measurement. We observed a level at 8049 keV. The angular distribution we extracted is compatible with a combination of $\ell_n = 0 + 2$ transitions, indicating it might be the combined peak of the nearby 8003 and 8082 keV levels, respectively.

*8174 keV level*. This level was only weakly populated in our measurement and an angular distribution could not be extracted. It was only observed previously in a $^{29}$Si($^3$He,$n$)$^{31}$S study [22].

*8328 keV level*. This level was previously observed by Davidson *et al*. [22] in their $^{29}$Si($^3$He,$n$)$^{31}$S study, and by Kankainen *et al*. [25] in their $^{31}$Cl $\beta$-decay study. Spin and parity values, however, are unknown.

*8462 keV level*. This level was previously observed in a number of studies [14,22,25]. It was assigned with $J^\pi = 13/2^-$ by Jenkins *et al*. [14] in their $^{12}$C($^{20}$Ne,$n\gamma$)$^{31}$S study.

*8515 keV level*. The 8515 keV level was reported recently by Kankainen *et al*. [25] ($E_x = 8509 \pm 30$ keV) via a $^{31}$Cl $\beta$-decay study. The angular distribution extracted in our measurement is compatible with an $\ell_n = 0$ transfer leading to an assignment of $J^\pi = 1/2^+$.

*8669, 8821, and 8977 keV levels*. These three levels have only been reported previously by Kankainen *et al*. [25] in their $^{31}$Cl $\beta$-decay study without spin and parity assignments.

*8789 keV level*. This level has not been reported previously. Our extracted angular distribution was best fit by an $\ell_n = 2$ transfer which allows $J^\pi = (3/2, 5/2)^+$.

*9154 and 10146 keV levels*. These two levels were observed by Jenkins *et al*. [14]. The 9154 keV level was assigned with $J^\pi = 13/2^+$ and the 10 146 keV level with $J^\pi = 13/2^-$, respectively.

*9423 keV level*. Källne and Fagerström reported a level at $9430 \pm 100$ keV in their $^{32}$S$(p, d)^{31}$S study [30]. The angular distribution we extracted is compatible with an $\ell_n = 2$ transition which allows $J^\pi = (3/2, 5/2)^+$; however, we could not rule out the possibility of an $\ell_n = 3$ transfer.

*9207, 9606, 9853, and 10577 keV levels*. These levels have not been previously reported. They were weakly populated in our measurement and angular distributions could not be extracted.

## IV. ASTROPHYSICAL IMPLICATIONS

The $^{30}$P$(p, \gamma)^{31}$S reaction rate has been found to have a pivotal role in nova nucleosynthesis in the heavier Si-Ca mass region [2,8,9]. Having combined results from our $^{32}$S$(p, d)^{31}$S measurement with previous results, we determine the properties of the levels within 1 MeV above the proton threshold in $^{31}$S (Table III) and calculate a new $^{30}$P$(p, \gamma)^{31}$S reaction rate.

Single-particle proton widths are calculated using a Woods-Saxon potential with $r = 1.25$ fm and diffuseness $a = 0.65$ fm. They are then converted into proton widths using spectroscopic factors. The spectroscopic factors as well as the $\gamma$ widths are taken from Ref. [15]. For the 6263 and 6350 keV states, we use spectroscopic factors obtained by Jenkins *et al*. [15] from an *sd* shell model calculation. For states where the spectroscopic factor is unknown, a value of 0.02 was assumed based on an investigation of the typical proton spectroscopic factors for states at similar excitation energies in mirror nuclei $^{31}$P [15,31]. The $\gamma$ widths are ignored for the first six resonances above the proton threshold, since $\Gamma_p \ll \Gamma_\gamma$. For the higher lying resonances, the $\gamma$ widths are obtained from the lifetimes of the mirror $^{31}$P states if known. For the higher lying low-spin, negative parity states, a typical $\gamma$ width derived from the 4 fs lifetime of the $3/2^-$ state at 6909 keV in $^{31}$P was used [15]. We neglect the states at 6279 and 7006 keV since we do not expect significant contribution to the $^{30}$P$(p, \gamma)^{31}$S rate from these $T = 3/2$ states by proton captures on a $T = 0$ ground state of $^{30}$P.

Using these resonance parameters in Table III, a new $^{30}$P$(p, \gamma)^{31}$S reaction rate was obtained and plotted in Fig. 4. The reaction rate for temperatures typical of nova is clearly dominated by two resonances at 6263 keV ($E_{\text{c.m.}} = 130$ keV) and 6544 keV ($E_{\text{c.m.}} = 411$ keV), the former at low temperatures and the latter at temperatures above 0.2 GK. For even lower temperatures below 0.03 GK, the rate is completely dominated by the 6160 keV ($E_{\text{c.m.}} = 27$ keV) resonance. The total rate is compared with that from Hauser-Feschbach calculations [11] and that obtained by Jenkins *et al*. [15] in the bottom panel of Fig. 4. For temperatures greater than 0.3 GK, the present rate agrees well with the Hauser-Feschbach rate, the difference is within a factor of 2. However at temperatures below 0.3 GK, including peak nova temperatures, our rate differs from the Hauser-Feschbach rate by a factor of up to 10. At even lower temperatures, the present rate differs from the Hauser-Feschbach rate by orders of magnitude. This shows that the statistical model is not valid at lower temperatures, as the rate is completely dominated by the individual low energy resonances. Our rate, however, agrees well with that obtained by Jenkins *et al*. [15] throughout the temperature range of nova interest with only a small difference due to updating the 6263 keV level resonance energy.

TABLE III. Summary of resonance properties within 1 MeV above the proton threshold used to calculate the $^{30}$P$(p,\gamma)^{31}$S reaction rate. $E_r$ is the resonance energy with respect to the $p+^{30}$P threshold at 6133 keV. $\Gamma_{sp}$ is the single-particle proton width. $C^2S$ is the spectroscopic factor for the $p+^{30}$P system in $^{31}$S, and $\omega\gamma$ is the resonance strength.

| $E_x$ (keV) | $E_r$ (keV) | $\ell_p$ | $\Gamma_{sp}$ (keV) | $C^2S$ | $\Gamma_p$(keV) | Lifetime (fs) | $\Gamma_\gamma$ (keV) | $\omega\gamma$ (keV) |
|---|---|---|---|---|---|---|---|---|
| 6160.2 | 27.2 | 1 | $1.02\,^{+2.10}_{-0.70}\times10^{-32}$ | 0.02 | $2.03\,^{+4.21}_{-1.40}\times10^{-34}$ | | | $2.03\,^{+4.21}_{-1.40}\times10^{-34}$ |
| 6263 | 130 | 0 | $6.89\,^{+4.02}_{-2.61}\times10^{-11}$ | 0.003 | $2.07\,^{+1.21}_{-0.78}\times10^{-13}$ | | | $7.16\,^{+4.18}_{-2.71}\times10^{-14}$[a] |
| 6263 | 130 | 2 | $5.50\,^{+3.24}_{-2.09}\times10^{-13}$ | 0.015 | $8.25\,^{+4.86}_{-3.14}\times10^{-15}$ | | | $2.75\,^{+1.62}_{-1.05}\times10^{-15}$ |
| 6350 | 217 | 2 | $5.68\,^{+6.66}_{-3.22}\times10^{-9}$ | 0.044 | $2.50\,^{+2.93}_{-1.42}\times10^{-10}$ | | | $2.50\,^{+2.93}_{-1.42}\times10^{-10}$ |
| 6376.9 | 243.9 | 3 | $7.75\,^{+0.25}_{-0.24}\times10^{-10}$ | 0.02 | $1.55\,^{+0.05}_{-0.05}\times10^{-11}$ | | | $2.58\,^{+0.08}_{-0.08}\times10^{-11}$ |
| 6393.8 | 260.8 | 4 | $2.12\,^{+0.06}_{-0.06}\times10^{-11}$ | 0.02 | $4.23\,^{+0.13}_{-0.12}\times10^{-13}$ | | | $8.46\,^{+0.25}_{-0.24}\times10^{-13}$ |
| 6544 | 411 | 1 | $4.55\,^{+1.27}_{-1.02}\times10^{-4}$ | 0.02 | $9.11\,^{+2.53}_{-2.04}\times10^{-6}$ | 3.9 | $1.69\times10^{-4}$ | $8.64\,^{+2.25}_{-1.86}\times10^{-6}$ |
| 6593 | 460 | 1 | $1.58\,^{+0.65}_{-0.48}\times10^{-3}$ | 0.02 | $3.17\,^{+1.29}_{-0.96}\times10^{-5}$ | 3.9 | $1.69\times10^{-4}$ | $1.78\,^{+0.57}_{-0.48}\times10^{-5}$ |
| 6636.2 | 503.2 | 3 | $9.68\,^{+0.33}_{-0.32}\times10^{-6}$ | 0.02 | $1.94\,^{+0.06}_{-0.06}\times10^{-7}$ | 202 | $3.26\times10^{-6}$ | $3.05\,^{+0.10}_{-0.09}\times10^{-7}$ |
| 6712 | 579 | 1 | $1.63\,^{+0.32}_{-0.28}\times10^{-2}$ | 0.02 | $3.26\,^{+0.64}_{-0.55}\times10^{-4}$ | 3.9 | $1.69\times10^{-4}$ | $7.42\,^{+0.44}_{-0.48}\times10^{-5}$ |
| 6748 | 615 | 1 | $2.88\,^{+0.46}_{-0.41}\times10^{-2}$ | 0.02 | $5.76\,^{+0.92}_{-0.81}\times10^{-4}$ | 3.9 | $1.69\times10^{-4}$ | $8.71\,^{+0.28}_{-0.31}\times10^{-5}$ |
| 6796 | 663 | 1 | $5.70\,^{+2.20}_{-1.66}\times10^{-2}$ | 0.02 | $1.14\,^{+0.44}_{-0.33}\times10^{-3}$ | 3.9 | $1.69\times10^{-4}$ | $9.81\,^{+0.37}_{-0.50}\times10^{-5}$ |
| 6833.4 | 700.4 | 5 | $5.21\,^{+0.03}_{-5.20}\times10^{-8}$ | 0.02 | $1.04\,^{+0.01}_{-1.04}\times10^{-9}$ | 123 | $5.37\times10^{-6}$ | $2.08\,^{+0.01}_{-2.08}\times10^{-9}$ |
| 6870 | 737 | 1 | $1.42\,^{+0.17}_{-0.16}\times10^{-1}$ | 0.02 | $2.85\,^{+0.34}_{-0.31}\times10^{-3}$ | 3.9 | $1.69\times10^{-4}$ | $1.06\,^{+0.01}_{-0.01}\times10^{-4}$ |
| 6921 | 788 | 2 | $2.38\,^{+0.73}_{-0.58}\times10^{-2}$ | 0.02 | $4.77\,^{+1.46}_{-1.16}\times10^{-4}$ | 3.9 | $1.69\times10^{-4}$ | $1.25\,^{+0.08}_{-0.10}\times10^{-4}$ |
| 6970 | 837 | 0 | $2.29\,^{+0.10}_{-0.10}$ | 0.02 | $4.58\,^{+0.21}_{-0.20}\times10^{-2}$ | 3.9 | $1.69\times10^{-4}$ | $5.61\,^{+0.00}_{-0.00}\times10^{-5}$ |
| 7038 | 905 | 2 | $7.54\,^{+0.27}_{-0.26}\times10^{-2}$ | 0.02 | $1.51\,^{+0.05}_{-0.05}\times10^{-3}$ | 3.9 | $1.69\times10^{-4}$ | $1.52\,^{+0.01}_{-0.01}\times10^{-4}$ |
| 7112 | 979 | 1 | $1.31\,^{+0.26}_{-0.22}$ | 0.02 | $2.61\,^{+0.52}_{-0.45}\times10^{-2}$ | 3.9 | $1.69\times10^{-4}$ | $5.60\,^{+0.01}_{-0.01}\times10^{-5}$ |
| 7155 | 1022 | 2 | $1.97\,^{+0.06}_{-0.06}\times10^{-1}$ | 0.02 | $3.94\,^{+0.12}_{-0.12}\times10^{-3}$ | 3.9 | $1.69\times10^{-4}$ | $1.62\,^{+0.01}_{-0.00}\times10^{-4}$ |

[a]Sum of contributions from $\ell_p=0$ and $\ell_p=2$ transfers.

We explored the uncertainties in the reaction rate arising from the uncertainties in the resonance energies and from the spectroscopic factors. We found that the reaction rate is reduced by a factor of 2 at $T_9=0.1$ when adopting the lower limits on the resonance energies and scaling the proton widths accordingly, while the upper limits on the resonance energies lead to a factor of 2 increase. The total variation is therefore roughly a factor of 4. This relatively small uncertainty in the reaction rate is primarily due to the improvement of the uncertainties in the resonance energies. To explore the uncertainties in the reaction rate arising from the spectroscopic factors, we arbitrarily varied the spectroscopic factors from 0 to 3 times the nominal values. We found that by setting individual spectroscopic factors to zero, the reaction rate could be reduced by as much as a factor of 20 at $T_9=0.1$, while the largest increase obtained was a factor of 5 when setting all of the spectroscopic factors to their largest values. Thus the total variation is approximately two orders of magnitude (see Fig. 4).

Expressions for the relevant nuclear reaction rates as analytic functions of the stellar temperature are crucial input for modeling complex astrophysical events such as novae. We have parametrized our new $^{30}$P$(p,\gamma)^{31}$S reaction rate using the online Computational Infrastructure for Nuclear Astrophysics [32]. The total reaction rate was fitted over the temperature range $0.03\leqslant T\leqslant 10.0$ GK. The residuals of the fit are less than 1% for most of the temperatures. A set of parameters of the REACLIB format [11] were obtained. The rate expression using these parameters is given in Table IV.

TABLE IV. Fit results and reaction rate expression for the $^{30}$P$(p,\gamma)^{31}$S rate. The reaction rate $N_A\langle\sigma v\rangle$ is in units of (cm$^3$ mole$^{-1}$ s$^{-1}$) and temperature $T_9$ in units of GK.

$$N_A\langle\sigma v\rangle = \exp(a_1 + a_2/T_9 + a_3/T_9^{1/3} + a_4T_9^{1/3} + a_5T_9 + a_6T_9^{5/3} + a_7\ln(T_9)) + \exp(a_8 + a_9/T_9 + a_{10}/T_9^{1/3} + a_{11}T_9^{1/3} + a_{12}T_9 + a_{13}T_9^{5/3} + a_{14}\ln(T_9))$$

| Parameter | | Fit result |
|---|---|---|
| $a_1$ | = | $2.43866\times10^{1}$ |
| $a_2$ | = | $-8.98316\times10^{0}$ |
| $a_3$ | = | $1.56029\times10^{2}$ |
| $a_4$ | = | $-1.74377\times10^{2}$ |
| $a_5$ | = | $7.46440\times10^{0}$ |
| $a_6$ | = | $-3.42232\times10^{-1}$ |
| $a_7$ | = | $9.92579\times10^{1}$ |
| $a_8$ | = | $-7.75663\times10^{3}$ |
| $a_9$ | = | $1.05093\times10^{1}$ |
| $a_{10}$ | = | $-1.99951\times10^{3}$ |
| $a_{11}$ | = | $1.18865\times10^{4}$ |
| $a_{12}$ | = | $-2.66872\times10^{3}$ |
| $a_{13}$ | = | $3.54294\times10^{2}$ |
| $a_{14}$ | = | $-2.90045\times10^{3}$ |

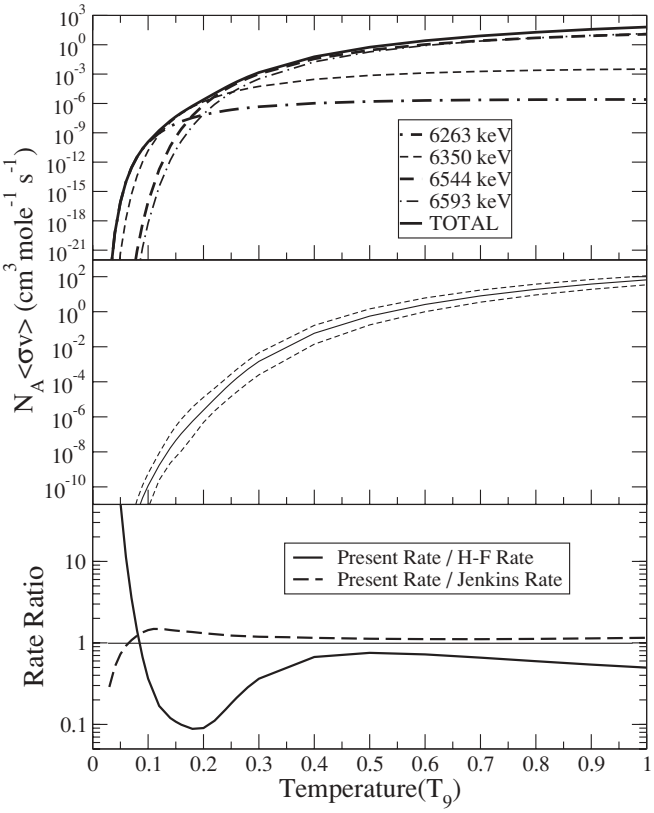


FIG. 4. $^{30}$P$(p,\gamma)^{31}$S reaction rate from present work (top panel). Contributions from individual resonances are also shown. Middle panel shows the uncertainties in the reaction rate arising from the uncertainties in the resonance energies and arbitrary variations of the spectroscopic factors (from 0 to 3 times the nominal values, see text). Bottom panel shows the ratio of reaction rate from present work to the rate from Hauser-Feschbach calculations and to that obtained by Jenkins *et al*. [15].

Using these new parameters, we have performed [32] multi-zone post-processing nucleosynthesis simulations of nova outbursts on 1.25 and 1.35 solar mass ONe white dwarfs and a 1.00 solar mass CO white dwarf (similar to Parete-Koon *et al*. 2003 [33]). The resulting abundance patterns reveal that production of some heavier elements in the Si-Ca mass region are altered by factors as large as 40% with respect to values found with the Hauser-Feschbach reaction rate. Enhancement of heavier elements production is also observed in our simulations. For example with respect to solar values, $^{31}$P shows overproduction factors of 1000 and 2600 in the 1.25 and 1.35 models, respectively. Significant enhancements are also seen for $^{28}$Si (50, 35), $^{29}$Si (50, 140), $^{30}$Si (550, 850), $^{32}$S (25, 23), and $^{35}$Cl (20, 1000) for example. Important constraints on nova models from specific isotopic ratios such as $^{12}$C/$^{13}$C, $^{14}$N/$^{15}$N and $^{26}$Al/$^{27}$Al are found to agree well with observed values in presolar grains that are believed to have nova origins [7]. Of special interest are the simulation results on silicon isotopic ratios in a typical 1.25 solar mass ONe white dwarf nova. We found that the $^{29}$Si/$^{28}$Si ratio is about equal to solar value. The $^{30}$Si/$^{28}$Si ratio, however, is about 12 times larger than the solar abundance ratio. This provides strong support that such grains are in fact of nova origin. Detailed results of these simulations, and additional effects on nova nucleosynthesis will be presented in a future paper.

## V. SUMMARY

In summary, we have measured the energy and angular distributions of deuterons from the $^{32}$S$(p,d)^{31}$S reaction. A total of 26 states in $^{31}$S were observed, 5 of which have not been reported previously. Uncertainties in the excitation energies for some levels were significantly reduced. Spins and parities of 15 levels in $^{31}$S were determined or constrained. We evaluated a total of 66 levels in $^{31}$S and used the new properties to calculate a new $^{30}$P$(p,\gamma)^{31}$S reaction rate. The resonance at 6263 keV is found to dominate the $^{30}$P$(p,\gamma)^{31}$S rate at lower temperatures in nova, while the state at 6544 keV dominates above 0.2 GK.

Although we have considerably improved the experimental information on the $^{31}$S level scheme above the proton threshold and the $^{30}$P$(p,\gamma)^{31}$S reaction rate, there are still significant uncertainties affecting calculations of the $^{30}$P$(p,\gamma)^{31}$S rate, as some parameters have come from theoretical determinations or estimations or information from the mirror $^{31}$P levels, and there still may be missing levels unaccounted for. Obtaining a $^{30}$P beam is therefore desirable for a direct measurement of the $^{30}$P$(p,\gamma)^{31}$S reaction rate.

## ACKNOWLEDGMENTS

The authors wish to thank D. G. Jenkins for useful discussions. The authors also thank the staff of the HRIBF whose hard work made this experiment possible. This research was supported by various grants from the U.S. Department of Energy and the National Science Foundation. Oak Ridge National Laboratory is managed by UT-Battelle, LLC, for the U.S. Department of Energy under Contract DE-AC05-00OR22725.

[1] J. José and M. Hernanz, Astrophys. J. **494**, 680 (1998).
[2] J. José *et al*., Astrophys. J. **560**, 897 (2001).
[3] J. Andreä, H. Drechsel, and S. Starrfield, Astron. Astrophys. **291**, 869 (1994).
[4] K. M. Vanlandingham, S. Starrfield, and S. N. Shore, Mon. Not. R. Astron. Soc. **290**, 87 (1997).
[5] M. D. Leising and D. D. Clayton, Astrophys. J. **323**, 159 (1987).
[6] A. Coc, M. G. Porquet, and F. Nowacki, Phys. Rev. C **61**, 015801 (2000).
[7] S. Amari *et al*., Astrophys. J. **551**, 1065 (2001).
[8] C. Iliadis *et al*., Astrophys. J. Suppl. Ser. **142**, 105 (2002).
[9] Z. Ma *et al*., American Astronomical Society Meeting 202, Abstract #30.02, (2003).
[10] W. R. Hix and F.-K. Thielemann, J. Comp. Appl. Math. **109**, 321 (1999).

[11] T. Rauscher and F.-K. Thielemann, At. Data Nucl. Data Tables **75**, 1 (2000).
[12] C. Iliadis *et al*., Astrophys. J. Suppl. Ser. **134**, 151 (2001).
[13] P. M. Endt, Nucl. Phys. **A633**, 1 (1998), and references therein.
[14] D. G. Jenkins *et al*., Phys. Rev. C **72**, 031303(R) (2005).
[15] D. G. Jenkins *et al*., Phys. Rev. C **73**, 065802 (2006).
[16] D. W. Bardayan *et al*., Phys. Rev. C **65**, 032801(R) (2002).
[17] D. W. Bardayan *et al*., Phys. Rev. C **62**, 055804 (2000).
[18] P. R. Bevington, *Data Reduction and Error Analysis for the Physical Sciences* (McGraw-Hill, New York, 1969).
[19] D. K. Olsen *et al*., Nucl. Instrum. Methods Phys. Res. A **254**, 1 (1987).
[20] F. Ajzenberg-Selove and J. L. Wiza, Phys. Rev. **143**, 853 (1966).
[21] T. S. Bhatia, W. W. Daehnick, and G. J. Wagner, Phys. Rev. C **5**, 111 (1972).
[22] J. M. Davidson *et al*., Nucl. Phys. **A240**, 253 (1975).
[23] C. E. Moss, Nucl. Phys. **A145**, 423 (1970).
[24] J. Vernotte *et al*., Nucl. Phys. **A655**, 415 (1999).
[25] A. Kankainen *et al*., Eur. Phys. J. A **27**, 67 (2006).
[26] R. L. Kozub, Phys. Rev. **172**, 1078 (1968).
[27] P. D. Kunz, http://spot.colorado.edu/∼kunz/
[28] H. Nann and B. H. Wildenthal, Phys. Rev. C **19**, 2146 (1979).
[29] J. Aysto, X. J. Xu, D. M. Moltz, J. E. Reiff, J. Cerny, and B. H. Wildenthal, Phys. Rev. C **32**, 1700 (1985).
[30] J. Källne and B. Fagerström, Phys. Scr. **11**, 79 (1975).
[31] J. Vernotte *et al*., Phys. Rev. C **41**, 1956 (1990).
[32] M. S. Smith *et al*., http://nucastrodata.org
[33] S. Parete-Koon *et al*., Astrophys. J. **598**, 1239 (2003).